# Heat Source Properties of Helium Gas Tungsten Arc with Metal Vapor[†]

TASHIRO Shinichi *, TANAKA Manabu ** and Kazuhiro NAKATA ***,

## Abstract

*The energy source characteristics of the gas tungsten arc (GTA) strongly depend on the physical property of the arc plasma. In welding processes, it has been experimentally confirmed that metal vapor evaporated from a high temperature weld pool drastically changes the property of the arc plasma and decreases its temperature. However, the effect of metal vapor on the characteristics of heat flux into a base metal is still not clear due to difficulties in experimental studies of arc plasmas. In this paper, the energy source property of helium GTA mixed with metal vapor was numerically analyzed. It was found that the intense radiation generated from dense metal vapor decreases the heat flux into a base metal and contracts the current density distribution, especially near the arc axis.*

## 1. Introduction

In an arc welding process such as gas metal arc (GMA), it has been experimentally confirmed that a large quantity of metal vapor evaporated from a weld pool and high temperature metal droplets at the tip of a welding wire drastically changes the physical property such as electrical conductivity of the arc plasma. The mixture of metal vapor decreases the temperature of arc plasma resulting in the reduction of heat flux into a base metal. Therefore it is important to understand the effect of the mixture of metal vapor on the arc welding process to improve the efficiency of welding.

A number of experimental investigations of the temperature distribution of arc plasma mixed with metal vapor in gas tungsten arc (GTA) have been conducted. For example, the plasma spectroscopic observation of argon (Ar) GTA [1,2] and nitrogen ($N_2$) GTA [3] revealed that the mixture of metal vapor increases the electrical conductivity of arc plasma and that the temperature consequently decreases by approximately 2,000K in the vicinity of the anode (the weld pool) in comparison with the cases of pure Ar and pure $N_2$ GTA. Recently, helium

(He) GTA using SUS304 as a base metal was also investigated and it was found that the mixture ratio of metal vapor reaches a level of 5% and the temperature decreases by approximately 6,000K near the fringe of the arc column [4-6]. On the other hand, it was also reported that the mixture hardly affects the temperature distribution in high arc current welding since metal vapor is swept away by strong cathode jets [7]. The computation analysis of Ar GTA with the mixture of copper [8] and iron [9] vapor was conducted using a magnetic-hydrodynamic modeling and it was found that the temperature decreases by 2,000K near the anode in comparison with the case of pure Ar GTA.

In contrast to the above phenomena, it is well known that a large quantity of metal vapor is generated from not only a weld pool but also from metal droplets at the tip of a wire in the case of GMA. **Figure 1** shows the photographs of He GTA [4-6] and He GMA. It is obvious that the most part of the arc column in the He GTA appears purple characteristic of pure He plasma because the mixture of metal vapor is limited to the anode (molten weld pool). On the contrary, metal vapor is mixed in

the entire arc column in GMA and the arc column becomes blue characteristic of a metal vapor plasma. It is thus expected that the influence of the metal vapor mixture on the plasma property is more significant in GMA than GTA. In GMA, not only the plasma phenomenon but also the droplet formation at the tip of a wire have to be considered and thus, highly sophisticated modeling is required. Recently several simulation models for GMA have been developed [10-13]. However, the effect of the metal vapor mixture has not been considered yet.

This study avoided the analyzing of complex phenomena such as formation, break away and transfer of droplets and assumed that a large quantity of metal vapor is mixed uniformly in the entire arc plasma as observed in GMA. The plasma property of He GTA is numerically analyzed as a virtual experiment and the results of the evaluation of the characteristics of heat flux into the anode are reported. A water-cooled copper anode was employed as a base metal since it was confirmed to be suitable in evaluating the heat flux characteristics [14]. In addition, only iron vapor was assumed as the mixture component for simplicity.

## 2. Simulation model

**Figure 2** shows the calculation region representing GTA that consists of a tungsten cathode with diameter of 3.2mm and tip angle of 60 degrees, arc plasma and a water-cooled copper anode. It is described in a frame of cylindrical coordinates with axial symmetry around the arc axis. The lengths of A-C and A-F are 45mm and 25mm, respectively. The electrode gap is set to be 5mm. The constant arc current of 150A is given inside the cathode. The shielding gas is introduced from the upper boundary at the flow rate of 10 l min$^{-1}$. As explained in the introduction, it is obvious that a large amount of metal vapor is mixed in the arc plasma of GMA compared with the GTA. In this study, the cases of the mixture ratios of 5%, 10% 20% and 30% which are higher than those examined in the previous study [6] are investigated in addition to pure He GTA. The laminar flow is assumed, and the arc plasma is considered to be in local thermodynamic equilibrium (LTE). The other numerical modeling methods are given in detail in our previous papers [15,16] which were extended from the Lowke's work [17]. The differential equations (1)-(6) are solved iteratively by the SIMPLEC numerical procedure [18].
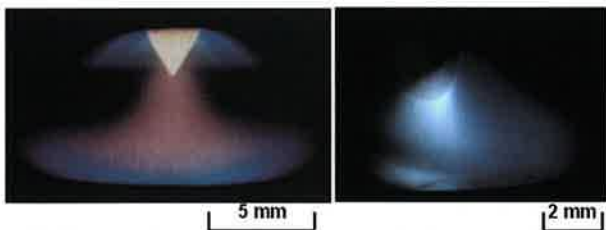


**Fig. 1** Photographs of GTA and GMA welding with pure He at arc current of 150A.
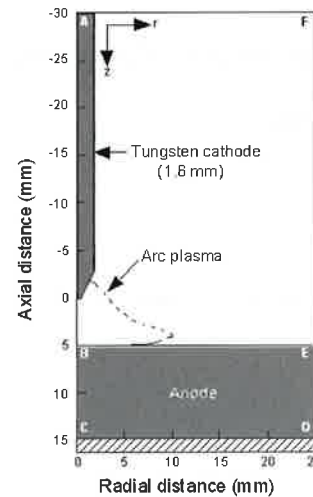


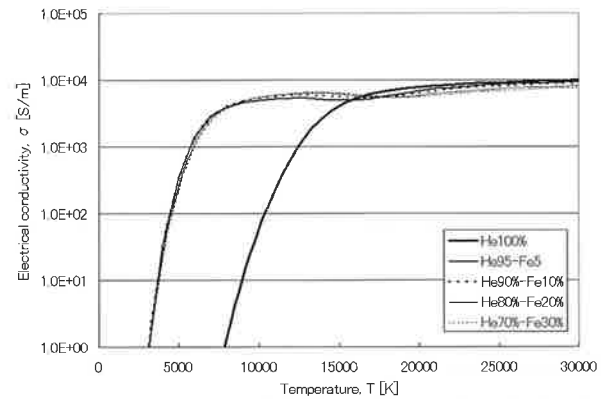**Fig. 2** Schematic illustration of numerical simulation region.



**Fig. 3** Temperature dependence of electrical conductivity for each mixture ratio.
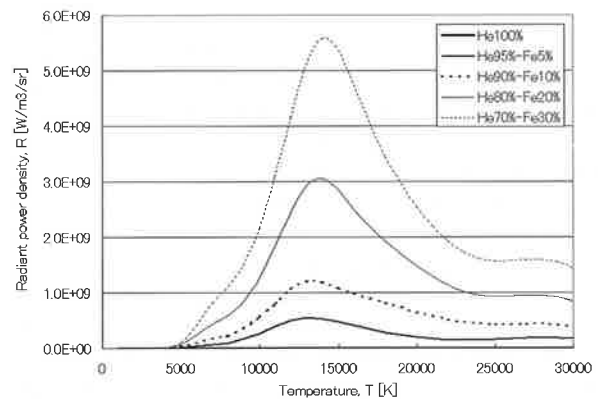


**Fig. 4** Temperature dependence of radiant power density for each mixture ratio.

The governing equations, boundary conditions and numerical method have been detailed in our previous papers [5, 6], so that only the most pertinent points are

explained here.

The mass continuity equation (1) is

$$\frac{1}{r}\frac{\partial}{\partial r}(r\rho v_r) + \frac{\partial}{\partial r}(\rho v_z) = 0$$

the radial momentum conservation equation (2) is

$$\frac{1}{r}\frac{\partial}{\partial r}(r\rho v_r^2) + \frac{\partial}{\partial z}(\rho v_z v_r) = -\frac{\partial P}{\partial r} - j_z B_\theta$$
$$+ \frac{1}{r}\frac{\partial}{\partial r}(2r\eta\frac{\partial v_r}{\partial r}) + \frac{\partial}{\partial z}(\eta\frac{\partial v_r}{\partial z} + \eta\frac{\partial v_z}{\partial r}) - 2\eta\frac{v_r}{r^2}$$

the axial momentum conservation equation (3) is

$$\frac{1}{r}\frac{\partial}{\partial r}(r\rho v_r v_z) + \frac{\partial}{\partial z}(\rho v_z^2) = -\frac{\partial P}{\partial z} + j_r B_\theta$$
$$+ \frac{\partial}{\partial z}(2\eta\frac{\partial v_z}{\partial z}) + \frac{1}{r}\frac{\partial}{\partial r}(r\eta\frac{\partial v_r}{\partial z} + r\eta\frac{\partial v_z}{\partial r})$$

the energy conservation equation (4) is

$$\frac{1}{r}\frac{\partial}{\partial r}(r\rho v_r h) + \frac{\partial}{\partial z}(\rho v_z h) = \frac{1}{r}\frac{\partial}{\partial r}(\frac{r\kappa}{c_p}\frac{\partial h}{\partial r}) + \frac{\partial}{\partial z}(\frac{\kappa}{c_p}\frac{\partial h}{\partial z})$$
$$+ j_r E_r + j_z E_z - R$$

the current continuity equation (5) is

$$\frac{1}{r}\frac{\partial}{\partial r}(rj_r) + \frac{\partial}{\partial z}(j_z) = 0$$

and the Ohm's law (6) is

$$j_r = -\sigma E_r ; j_z = -\sigma E_z$$

In the above equations, t is time, h is enthalpy, P is pressure, $v_z$ and $v_r$ are the axial and radial velocities, $j_z$ and $j_r$ are the axial and radial components of current density, g is acceleration due to gravity, $\kappa$ is thermal conductivity, $C_p$ is specific heat, $\rho$ is density, $\eta$ is viscosity, $\sigma$ is electrical conductivity, R is radiation emission coefficient, $E_r$ and $E_z$ are the radial and axial components of the electric field defined by $E_r = -\partial V/\partial r$ and $E_z = -\partial V/\partial z$, where V is electric potential. The azimuthal magnetic field $B_\theta$ induced by arc current is evaluated by the following Maxwell's equation (7):

$$\frac{1}{r}\frac{\partial}{\partial r}(rB_\theta) = \mu_0 j_z$$

where, $\mu_0$ is permeability in vacuum.

In order to solve the above equations (1) to (6), special condition about thermal flux that occurs only at the electrode surface must be considered. An additional energy flux term at the cathode surface is needed in equation (4) considering thermionic cooling due to the emission of electrons, ion heating, and radiation cooling. The additional energy flux for the cathode $H_k$ is defined as:

$$H_K = -\varepsilon\alpha T^4 - |j_e|\phi_K + |j_i|V_i \qquad (8)$$

where, $\varepsilon$ is surface emissivity, $\alpha$ is the Stefan-Boltzmann constant, $\phi_K$ is the work function of the tungsten cathode, $V_i$ is the ionization potential of argon, $j_e$ is electron current density, and $j_i$ is ion current density.

As to thermionic emission of electrons at the cathode surface, $j_e$ cannot exceed the Richardson current density $J_R$ [19] given by:

$$|j_R| = AT^2 \exp\left(-\frac{e\phi_e}{k_B T}\right) \qquad (9)$$

where, A is the thermionic emission constant for the cathode surface, $\phi_e$ is the effective work function for thermionic emission of the electrode surface at the local surface temperature, and $k_B$ is the Boltzmann's constant. The ion-current density $j_i$ is then assumed to be $|j|-|j_R|$ if $|j|$ is greater than $|j_R|$, where $|j|=|j_e|+|j_i|$ is total current density at the cathode surface obtained from equation (5)

Similarly, for the anode surface, equation (4) needs an additional energy flux term for heating by electron condensation (thermionic heating) and radiation cooling. The additional energy flux for the anode, $H_A$ is defined as:

$$H_A = -\varepsilon\alpha T^4 + |j|\phi_A \qquad (10)$$

where, $\phi_A$ is the work function of the anode and $|j|$ is current density at the anode surface obtained from equation (5). The term including $\phi_A$ accounts for heating of the anode by electrons, which deliver energy equal to the work function absorbed at the anode. This term is analogous to the cooling effect that occurs at the cathode when electrons are emitted.

The thermodynamic coefficients and transport coefficients are calculated based on the first-Chapman-Enskog approximation [20]. The radiation emission coefficients are given in the same manner as reported in the literature [21]. Metal vapor is characterized by its high electrical conductivity and high radiation emission coefficient. The temperature dependence of electrical conductivity and radiation emission coefficients, which is important for the analysis, is presented in **Figure 3** and **Figure 4**, respectively.

## 3. Results and Discussion

The simulation results of the distribution of temperature and fluid flow velocity of arc plasma are shown for pure He in **Figure 5**, for He-5% Fe in **Figure 6**, and for He-30% Fe in **Figure 7**. It is seen that the arc column tends to contract as the iron vapor mixture ratio increases and that the plasma temperature drastically decreases except in the vicinity of the cathode. In fact, the plasma temperature is decreased by 6,000K on the fringe of the arc column (r=2.0mm) and in the vicinity of the anode (z=4.0mm) when the mixture ratio of iron vapor is increased from 0% (pure He) to 5%. This simulation result is in well accordance with the experimental one [4]. On the other hand, in the vicinity of the cathode, both the maximum plasma temperature and the maximum cathode jet velocity are reduced below the levels in the case of pure He due to the mixture of iron vapor of 5%. However, these increase above the levels in the case of pure He when the mixture ratio is raised to 30%.

As a general characteristic of metal vapor, it raises electrical conductivity of the arc plasma and enhances radiation heat loss. In fact, only a small amount of metal vapor greatly raises electrical conductivity, because the ionization potential of iron vapor (7.9eV) is only a third of that of He (24.6eV). As shown in Fig. 3, this tendency becomes more significant in the lower temperature regions. The electrical conductivity of arc plasma mixed with metal vapor is more than ten times higher than that of pure He at temperatures less than 15,000K. Above this temperature, however, the electrical conductivity does not differ between with and without metal vapor. As to the radiation heat loss, it increases nearly in proportion to the mixture ratio because the radiation by He is negligible.
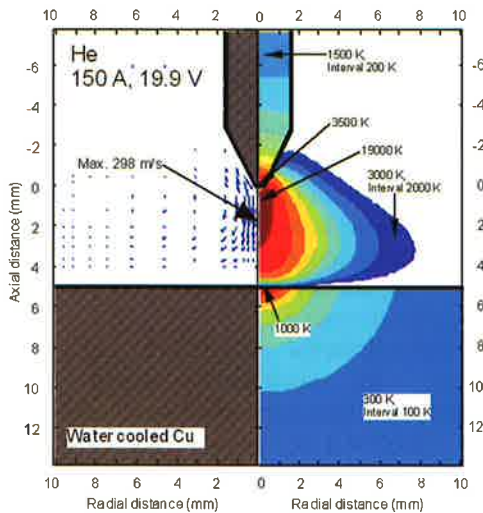


Fig. 5 Two-dimensional distribution of temperature and fluid flow velocity of arc plasma for pure He.
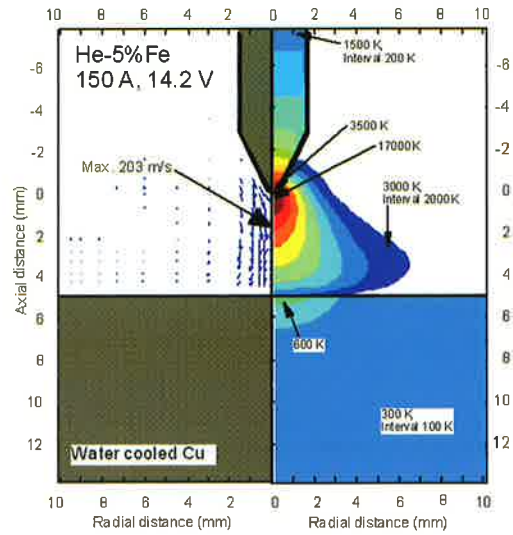


Fig. 6 Two-dimensional distribution of temperature and fluid flow velocity of arc plasma for He-5%iron.
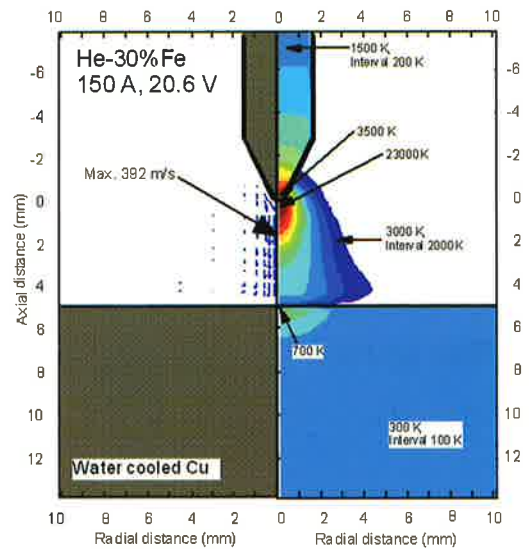


Fig. 7 Two-dimensional distribution of temperature and fluid flow velocity of arc plasma for He-30%iron.

The results on the radial distribution of current density at the anode surface is shown in **Figure 8**. It is found that in the relatively lower plasma temperature regions, except in the vicinity of the cathode, the mixture of iron vapor of 5% raises electrical conductivity within the wide radial directions and makes the current density distribution level off. As a result, the plasma temperature in this region decreases due to the radiation heat loss as well as to a decrease of Joule heat.

At the mixture ratio of 10% or higher, the current density distribution tends to contract in the vicinity of the

arc axis. Because an increase of electrical conductivity due to the mixture of iron vapor is saturated at the mixture ratio over 5% as shown in Fig. 3, the effect of the radiation heat loss becomes dominant. On the fringe of the arc column, electrical conductivity decreases due to a plasma temperature decrease caused by radiation heat loss. It follows that the current path is restricted in the vicinity of the arc axis and the current density distribution contracts due to a so-called thermal pinch effect.

For the same reason, at the high plasma temperature region near the cathode, an increase of electrical conductivity due to the mixture of iron vapor is negligibly small and thus the effect of radiation heat loss on the contraction of the current density distribution becomes dominant. It is considered that at higher mixture ratio the increase of current density caused by the contraction enhances Joule heating and raises plasma temperatures and that the electro-magnetic pinching force is strengthened at the same time so that the cathode jet is accelerated.

The result on the radial distribution of heat flux density to the anode surface is shown in **Figure 9**. The decrease of plasma temperatures in the vicinity of the anode reduces the thermal conduction to the anode surface and the electron condensation decreases in proportion to a decrease in the current density. As shown in Fig. 9, at the mixture ratio of 5%, the maximum heat flux density drops to 30% that of pure He. At the same time the temperature on the anode surface drastically decreases. At mixture ratios over 5%, the effect of radiation heat loss becomes dominant and current density distributions contract due to the same mechanism as a thermal pinch effect so that the heat flux density by electron condensation increases. As a result, the maximum heat flux density and the maximum anode surface temperature slightly increase as the mixture ratio increases over 5%.
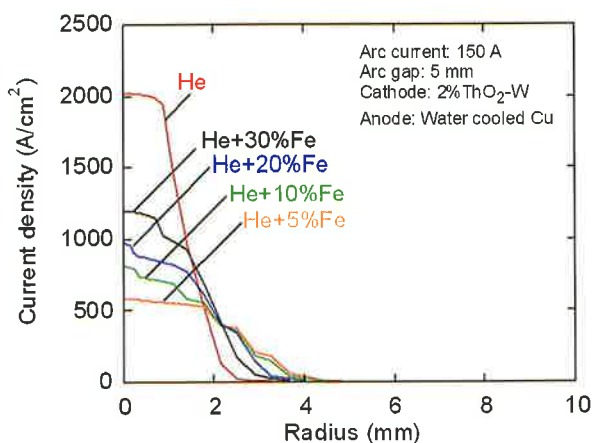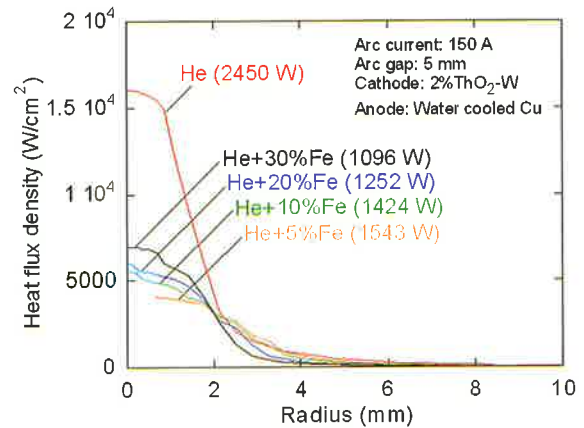


**Fig. 9** Radial distributions of heat flux density to the anode surface.

The calculated result on the iron vapor mixture dependence of input power, heat input to the anode and radiation heat loss is plotted against the left vertical axis and that of thermal efficiency of arc is plotted against the right vertical axis in **Figure 10**. As shown in Fig.10, the radiation heat loss increases nearly in proportion to the iron vapor mixture ratio. With an increase in this ratio, the plasma temperature in the vicinity of the anode decreases and thermal conduction to the anode also decreases. It follows that the heat input to the anode decreases in inverse proportion to the mixture ratio. At the mixture ratio less than 5%, the input power tends to decrease due to the increase of electrical conductivity but it increases at the mixture ratio over 5% in order to compensate the radiation heat loss. As a result, the thermal efficiency drastically decreases with an increase in the mixture ratio, reaching a level less than 50% at the mixture ratio of 30%.
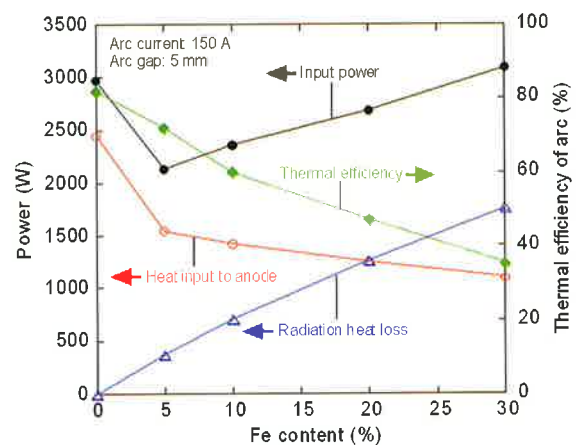


**Fig. 8** Radial distributions of current density on the anode surface.



**Fig. 10** Dependence of input power, thermal efficiency, heat input to the anode and radiation heat loss on iron vapor content.

## 4. Conclusions

A numerical analysis was conducted to investigate the arc plasma characteristics of He GTA with the mixture of iron vapor. The characteristics of the heat flux to the water-cooled copper anode were also analyzed. It was found that the effect of the mixture of metal vapor has to be taken into account in analyzing GMA phenomena. The important findings are as follows:

(1) Electrical conductivity increases and radiation heat loss is enhanced as the mixture ratio of iron vapor is increased. At the mixture ratio of 5%, the plasma temperature on the fringe of arc column and in the vicinity of the anode is reduced by 6,000K compared with the case of pure He.

(2) Radiation heat loss of arc plasma contracts arc column as well as the current density distribution, resulting in an increase of the maximum temperature of arc plasma.

(3) At the iron vapor mixture ratio of 5%, the maximum heat flux density to the anode lowers to 30% that of that at 0% ratio (pure He) and the maximum temperature on the anode surface drastically decreases. At the mixture ratios higher than 5%, both the maximum heat flux density and the anode surface temperature tend to increase.

(4) At the mixture ratio less than 5%, input power decreases due to the effect of an increase of electrical conductivity. However, at the mixture ratio over 5%, input power increases in order to compensate the radiation heat loss. As a result, thermal efficiency significantly decreases with increasing mixture ratio, becoming less than 50% at the mixture ratio of 30%.

### References

1) Etemadi K et al.; *Plasma Chem. Plasma Proc.*, 1985; 5: p175-182.

2) Razafinimanana M et al.; *Plasma Sources Sci. Technol.*, 1995; 4: p501-510.

3) Rahal AM et al.; *J. Phys. D: Appl. Phys.*, 1984; 17: p1807-1822.

4) Terasaki H et al.; *Metall. mater. trans. A*, 2002; 33A: p1183-1188.

5) Terasaki H et al.; *Journal of Welding Society*, 2002; 20: p201-206.

6) Terasaki H : *Master thesis, Osaka University*, Japan, 2000.

7) Farmer AJD et al.; *J. Phys. D: Appl. Phys.*, 1986; 19: p1723-1730.

8) Menart J et al.; *Plasma Chem. Plasma Process*, 1999; 19: p153-170.

9) Gonzalez JJ et al.; *J. Appl. Phys.*, 1993; 74: p3065-3070.

10) Fan HG et al.; *J. Phys. D: Appl. Phys.*, 2004; 37: p2531-2544.

11) Hirata Y et al.; *Preprints of the National meeting of JWS*, 2004; 22: p80-81 (in Japanese).

12) Quinn TP et al.; Sci. Technol. *Weld. Joining*, 2005; 10: p113-119.

13) Yamamoto T et al.; Sci. Technol. *Weld. Joining*, 2002; 7: p260-264.

14) Ushio M et al.; *IEEE Trans. Plasma Sci.*, 2004; 32: p108-117.

15) Tanaka M et.al.; *Metal. Trans. A*, 2002; 33A: p2043-2052.

16) Tanaka M et.al.; *Plasma Chem. Plasma Process*, 2003; 23: p585-606.

17) Lowke JJ et.al ; *J. Phys. D: Appl. Phys.*, 1997; 30: p1-10.

18) Patanker SV ; *Numerical Heat Transfer and Fluid Flow*, Hemisphere Publishing Corporation, 1980.

19) Pfender E; *Gaseous Electronics*, Academic Press, 1978.

20) Yos JM; *Transport Properties of Nitrogen, Hydrogen Oxygen, and Air to 30000 K*, Research and Advanced Development Division AVCO Corporation, 1963.

21) Honda S et.al.; *The papers of Technical Meeting on Frontier Technology and Engineering*, IEE Japan, 2005; 7: FTE-05-2.